

THE X-RAY SOURCE POPULATION OF “THE ANTENNAE” GALAXIES: X-RAY PROPERTIES FROM *CHANDRA* AND MULTIWAVELENGTH ASSOCIATIONS

A. ZEAS, G. FABBIANO, A. H. ROTS, S. S. MURRAY
 Harvard-Smithsonian Center for Astrophysics,
 60 Garden Street, Cambridge, MA 02138

Draft version October 30, 2018

ABSTRACT

We investigate the nature of the luminous X-ray source population detected in a (72 ks) *Chandra* ACIS-S observation of NGC 4038/39, the Antennae galaxies. We derive the average X-ray spectral properties of sources in different luminosity ranges, and we correlate the X-ray positions with radio, IR, and optical (*HST*) data. The X-ray sources are predominantly associated with young stellar clusters, indicating that they belong to the young stellar population. Based on both their co-added X-ray spectrum, and on the lack of associated radio emission, we conclude that the Ultra Luminous X-ray sources (ULXs), with $L_X \geq 10^{39} \text{ ergs s}^{-1}$, are not young compact Supernova Remnants (SNR), but accretion binaries. While their spectrum is consistent with those of ULXs studied in nearby galaxies, and interpreted as the counterparts of intermediate mass black-holes ($M > 10 - 1000 M_\odot$), comparison with the position of star-clusters suggests that some of the ULXs may be runaway binaries, thus suggesting lower-mass binary systems. The co-added spectrum of the sources in the $3 \times 10^{38} - 10^{39} \text{ erg s}^{-1}$ luminosity range is consistent with those of Galactic black-hole candidates. These sources are also on average displaced from neighboring star clusters. The softer spectrum of the less luminous sources suggests the presence of SNRs or of hot interstellar medium (ISM) in the *Chandra* source extraction area. Comparison with HI and CO observations shows that most sources are detected in the outskirts of large concentrations of gas. The absorbing columns inferred from these observations would indeed absorb X-rays up to 5 keV, so there may be several hidden X-ray sources. Associated with these obscured regions we find 6 sources with heavily absorbed X-ray spectra and absorption-corrected luminosities in the ULX range. We detect the nuclei of both galaxies with luminosities in the $10^{39} \text{ ergs s}^{-1}$ range and soft, possibly thermal, X-ray spectra.

Subject headings: galaxies: peculiar — galaxies: individual — galaxies: interactions — X-rays: galaxies

1. INTRODUCTION

X-ray studies of normal and actively star-forming galaxies with the *Einstein* Observatory and *ROSAT* suggested that their X-ray emission arises from a population of discrete sources (X-ray binaries, XRBs, and supernova remnants, SNRs), as well as from superwinds and hot ISM associated with starburst activity (for reviews see Fabbiano 1989, 1995). A few of the point-like sources were found to have extremely high X-ray luminosities, when compared to the analogous populations of the Milky Way or M31 (e.g., Fabbiano 1995). These luminosities are well in excess of the Eddington luminosity for an accreting neutron star and have led to speculations that the Ultra-Luminous X-ray sources (ULXs) may be associated with intermediate mass black holes ($10\text{--}100 M_\odot$; e.g., Fabbiano 1989, Zezas et al. 1999, Roberts & Warwick 2000, Makishima et al. 2000).

Although these studies suggested both variety and complexity in the X-ray source populations of galaxies, beyond what can be observed in our local environment, it is only now with the sub-arcsecond resolution of *Chandra* (Van Speybroeck et al. 1997; Weisskopf et al. 2000) that studies of galactic X-ray source populations can be attempted at large. With *Chandra* individual X-ray sources are not likely to be confused in observations of galaxies as far as the Virgo cluster and beyond. Moreover, the high spatial

resolution of *Chandra* results in very low background contamination, allowing the detection of very faint sources.

In this paper we discuss the nature of 49 luminous X-ray sources detected with *Chandra* in the actively star-forming merging galaxies NGC 4038/39 (*Chandra* Observation ID 315; see Fabbiano, Zezas & Murray 2001 for a first overall discussion of these data), by means of their average X-ray spectral properties and possible counterparts at different wavelengths. The detection of these sources and their detailed X-ray analysis is reported in Zezas et al (2002; Paper II). This population of X-ray sources is exceptional, because of the very large number of ULXs in a single galaxy.

The Antennae are the prototypical system of merging galaxies (Toomre & Toomre 1977), and a wealth of multi-frequency observational data are available. The system is in an early merging phase about 3×10^8 yr before full coalescence (Georgakakis et al. 2001), when intense bursts of star-formation are likely to occur (e.g. Mihos & Hernquist 1996). Optical and near-IR observations show that there are several generations of stellar populations with ages ranging from 6 Myr to ~ 1 Gyr (e.g. Whitmore et al. 1999, Kunze et al. 1996, Mengel et al. 2001, Fisher et al. 1996). In the mid-IR ($10\text{--}20 \mu\text{m}$), as well as in molecular CO, the dust-enshrouded contact region of the two merging galaxies, where most of the star formation is presently occurring, dominates the emission (Mirabel et al. 1998, Wilson

et al. 2001). A large number of both non-thermal (SNRs) and thermal (HII regions) radio sources are detected in VLA observations at 6 cm and 20 cm (Neff & Ulvestad 2000). Zhang et al. (2001) performed a multiwavelength study of the young star-clusters in the Antennae galaxies. They find that the youngest clusters (younger than 5 Myr) are associated preferentially with radio continuum, HI and CO emission whereas slightly older clusters (ages 5 - 160 Myr) are associated with H α , UV and X-ray emission (the latter based on ROSAT data).

This paper is organized as follows: in §2. we summarize the results of Paper II that are pertinent to the present discussion; in §3. we further investigate the properties of the X-ray source population, by analyzing the average spectral properties in different luminosity ranges; in §4. we obtain additional constraints to the nature and evolution of the X-ray sources, by examining their multi-wavelength environment; in §5 we discuss our result; our conclusions are summarized in §6. Throughout this paper we use a distance of 29 Mpc ($H_0 = 50 \text{ km s}^{-1} \text{ Mpc}^{-1}$). For $H_0 = 75 \text{ km s}^{-1} \text{ Mpc}^{-1}$, the distance becomes 19.3 Mpc and all the cited luminosities will be a factor of 2.25 lower. At a distance of 29 Mpc, 1 arcsec corresponds to a physical distance of 140 pc (at 19 Mpc it corresponds to 92 pc). All cited luminosities are in the 0.1-10.0 keV band, unless otherwise stated.

2. SUMMARY OF INDIVIDUAL X-RAY SOURCE PROPERTIES

We refer to Paper II (Zezas et al. 2002) for a detailed analysis of the discrete X-ray sources discovered with *Chandra* in the Antennae. Here we summarize the main results:

1) Forty-nine sources are detected down to a detection limit of $\sim 10^{38} \text{ erg s}^{-1}$ ($H_0 = 50 \text{ km s}^{-1} \text{ Mpc}^{-1}$; $5 \times 10^{37} \text{ erg s}^{-1}$ for $H_0 = 75 \text{ km s}^{-1} \text{ Mpc}^{-1}$). A soft (0.3 - 2.0 keV) and a medium (2.0- 4.0 keV) band image of the Antennae is presented in Figure 1. The detected sources are marked by the 3σ ellipses fit to the spatial distribution of the source events, and numbered following the numbering convention of Table 1 in Paper II. Only 6 of these sources, including the Southern nucleus and one source in the Northern nuclear region, are associated with small-scale extended X-ray emission (sources 5, 6, 7, 10, 24, 29; identified with light blue ellipses in Fig. 1); the other 43 sources appear point-like.

2) Of the 49 sources, 31 have luminosities below $\sim 10^{39} \text{ erg s}^{-1}$ ($H_0 = 50 \text{ km s}^{-1} \text{ Mpc}^{-1}$), while 18 are ULXs with absorption corrected luminosities ranging from $10^{39} \text{ erg s}^{-1}$ up to $2 \times 10^{40} \text{ erg s}^{-1}$, for a 5 keV Bremsstrahlung model and Galactic line-of-sight N_H .

3) There is some evidence of time variability in the ULXs: two sources (14, 44) are found to vary during the *Chandra* observation and 3 of the 6 sources for which a comparison with the 5" resolution *ROSAT HRI* observations (Fabbiano et al. 1997) is possible, were found to be variable (16, 42, 44/46) in timescales of years. These variable sources are identified by green ellipses in Fig. 1.

4) We fitted the data with both an absorbed power-law model and a thermal Raymond-Smith model with solar abundances and absorption. In most cases the power-law model favors column densities in excess of the Galactic line

of sight N_H , while the Raymond-Smith model requires much lower absorbing column densities, without significantly improving the fit. Two-component models (power-law plus Raymond Smith) were fitted to the spectra of 10 sources for which a large enough number of counts was detected. In all these fits, the overall N_H is consistent with the Galactic value, while the hard component has usually a higher absorption. Three sources show significant fit residuals suggesting the presence of emission lines.

5) Six sources have large best-fit column densities (greater than 10 times the line of sight Galactic N_H) in both the power-law and the double component spectral fits, suggesting truly absorbed spectra. These sources (12, 24, 25, 34, 35, 36) are identified by black ellipses in Fig. 1, and reside in or near the very dusty contact region of the two merging galaxies.

6) There is a suggestion both from the X-ray colors (Hardness Ratios) and the power-law slopes in the simple power-law fits, that more luminous sources tend to be harder. Photon indices range from $\Gamma \sim 1.2$ for the most luminous ULXs to $\Gamma > 3.0$ for fainter sources, but the uncertainties are very large in most cases, because of the limited statistics.

3. CO-ADDED X-RAY SPECTRA

Detailed observations of luminous X-ray sources in the Milky Way and Magellanic Clouds, augmented more recently by a few observations in nearby spirals galaxies, have produced a 'library' of spectral shapes characteristics of different types of sources, which in the case of accreting binaries may also depend on the intensity of the source at a given time. Pulsar XRBs as well as Black Hole (BH) binaries in low state tend to have hard spectra ($\Gamma < 2.0$; e.g. Nagase 1989, Tanaka & Lewin 1995). The spectra of BH binaries in high state and unmagnetised neutron stars are dominated by a multi-temperature disk black-body (disk-BB) spectrum (e.g. van Paradijs 1999, Tanaka & Lewin 1995). ULXs in nearby galaxies have also been found to oscillate between these intensity/spectral states (e.g. La Parola et al. 2001; Kubota et al. 2001). SNRs typically exhibit soft thermal emission (kT $\sim 0.5 - 5.0$ keV; e.g., Schlegel 1995), although young supernovae detonating in dense environments (cSNRs) can have much harder spectra (Plewa 1995, Terlevich 1994).

The general spectral trend found in Paper II for the sources in the Antennae suggests that the ULXs may resemble similarly hard ULXs found in other galaxies, which on the basis of their spectral behaviour were identified with accretion binaries (e.g. LaParola et al 2001). However, even for these sources the number of detected photons is not high enough to pursue a detailed spectral investigation. The situation is even harder for fainter sources.

For this reason we investigated the average spectral properties of sources in three different luminosity ranges, by extracting and analyzing co-added spectra for the sources in each group. The underlying assumption is that, in each luminosity range, the source population may be dominated by a given type of sources, so that the coadded spectrum may express the average spectral characteristics of these sources. While the conclusive work will require future deeper observations, this assumption is supported by the general characteristics of the Galactic X-ray sources

(e.g. Watson 1990) and by the general luminosity-spectral trend reported in Paper II.

In *Group 1* we included sources with $L_X < 3 \times 10^{38}$ erg s $^{-1}$ which is the Eddington luminosity for the upper range of neutron star masses. If $H_0 = 75$ km s $^{-1}$ Mpc $^{-1}$ this limit becomes 1.3×10^{38} erg s $^{-1}$, the Eddington luminosity for 1 M_\odot object. *Group 2* includes sources with luminosities between 3×10^{38} and 10^{39} erg s $^{-1}$ ($1.3 \times 10^{38} - 4 \times 10^{38}$ erg s $^{-1}$ for $H_0 = 75$ km s $^{-1}$ Mpc $^{-1}$), that may host stellar mass black holes, if the spherical accretion paradigm applies. *Group 3* includes the ULXs.

Co-adding spectra may introduce spurious features, mainly below 1.0 keV, due to the varying column density of the individual spectra. However, the spectral parameters we are interested in (the power-law photon index Γ , and the temperature of the accretion disk) mostly depend on the shape of the continuum above 1.0 keV. For the same reason, calibration uncertainties below 1.0 keV do not affect our conclusions. In order to account for these uncertainties, we include 10% systematic errors in the spectra of the brightest sources, in the region of the Oxygen edge (~ 0.5 keV). Because of variations of the intensity of the diffuse emission and of the area used to extract the source spectra, we cannot use the local background of each source, since the background spectrum will not be correctly normalized to the source area. Therefore, the background spectrum was taken from a large, source-free area around the galaxy. For this reason, the co-added spectra may contain some residual local diffuse emission. We analyzed these spectra following the procedures described in Paper II.

The coadded spectra, together with the best fit models and the fit residuals, are presented in Fig. 2. Because of the higher S/N of the co-added spectra we were able to fit a wider range of models to the data: single component power-law (PO) and optically thin thermal Raymond-Smith models (RS), a combination of PO and RS (PO+RS), a PO and a multi-temperature disk blackbody (PO + disk-BB), a PO+disk-BB with a thermal RS component (PO+RS+disk-BB) and finally a PO+RS+RS model. The results of the spectral fitting are given in Table 1A. The first column gives the source luminosity range of the co-added spectra, Columns (2) and (3) give the parameters of the PO fits (Γ and N_H in the first line and χ^2 and dof in the second line); Columns (4) and (5) give the parameters of the PO+RS model (Γ and kT in the first line and χ^2 in the second line); Columns (6) and (7) give the parameters of the PO + disk-BB model (Γ and the inner temperature of the disk, in the first line and the N_H and χ^2 (dof) in the second line); Columns (8) and (9) give the parameters of the PO + RS + disk-BB model fits (Γ and kT in the first line, inner temperature of the disk and N_H in the second line, and χ^2 in the third line); Columns (10) and (11) give the parameters of the PO + RS + RS model (Γ and kT in the first line, kT and N_H in the second line and χ^2 in the third line). All temperatures are in units of keV and the N_H is in units of 10^{22} cm $^{-2}$. The parameters of the best fit models are shown in boldface.

Single component models gave an unacceptable fit in all cases. Fits to composite PO+RS models gave an improved fit at more than 99% confidence level for 2 addi-

tional parameters. This composite model gave a very good fit for the spectrum of Group 1, but is still unacceptable for Groups 2 and 3. A composite PO + disk-BB model (that was found to represent well certain Galactic sources, and ULXs in nearby spirals, e.g. Kubota et al. 2001), in the case of Group 1, gave a fit of similar quality to the PO+RS model, but for Groups 2 and 3 the quality of the fit was still unacceptable. PO photon indices Γ tend to be large for fainter sources (Group 1) in agreement with the trends found in Paper II.

Including a third component (PO+RS+RS or PO+RS + disk-BB model) to fit the spectra of Groups 2 and 3, improved the fit in both cases. The PO+RS + disk-BB model gave a slightly improved the fit for Group 3. The best-fit power-laws are fairly hard, reaching values of $\Gamma \sim 1.5$ for the disk-BB model fits. In this model, the inner temperature of the accretion disk is higher for the ULXs, reaching values comparable to those reported by studies of individual ULX spectra with ASCA (Makishima et al 2000).

The residuals from these best fit models for groups 1 and 2 showed line-like features. We modeled these features by adding narrow gaussian lines to the models. Group 1 requires only one additional line at 1.3 keV corresponding Mg IX. Group 2 requires two lines, one at ~ 1.8 keV and another one at ~ 2.5 keV corresponding to the Si X - Si XIV triplet and S XIV, respectively. We note that using a double thermal model (RS+RS) does not improve the fit compared to both the PO+RS and the PO+RS+gauss models.

The overall best fit models are the PO+RS for Group 1, the PO+RS+RS (or PO+disk-BB+RS) for Group 2 and the PO+RS+disk BB (or PO+RS+RS) for Group 3. In Table 1B we give the relative contribution of each component to the soft (0.1-2.5) keV and hard (2.5-10.0) keV bands: Column (1) gives the luminosity range of the co-added spectra, Column (2) gives the spectral component, Columns (3) and (4) give the contribution of each component in the soft and hard band (normalized by the total flux in each band). The RS component contributes relatively more in the fainter X-ray sources, in agreement with the spectral softening reported in Paper II. However, this effect could also be due to the relatively larger contribution of the hot ISM of the Antennae (Paper I) to the spectral extraction areas of fainter point-like sources.

4. MULTIWAVELENGTH STUDY

The discrete source population of the Antennae tends to follow the areas where the H α emission is more intense (Paper I), suggesting a connection with the young stellar component. To better constrain the nature of these sources, we have also looked at their multi-wavelength emission environment, using publicly available data and papers in the literature. In particular, we have compared the X-ray positions with the star clusters discovered in the HST WFPC2 observations (Whitmore et al. 1995, 1999), to establish if our sources can be associated with a star cluster; we have compared our sources with the radio source lists of Neff & Ulvestad (2000), to establish if some of these may be associated with SNRs; comparisons with both HST and IR data (e.g., Mengel et al 2001) constrain the age of the associated stellar cluster, and therefore the age and evolution of the X-ray source; comparisons between the X-ray

absorption columns and HI and CO observations help to establish the 3-dimensional locations of these sources in the parent galaxies. The results of these comparisons are given below.

4.1. Optical

The Antennae galaxies have been extensively observed with the WFPC and the WFPC2 on board HST (Whitmore et al. 1995, 1999). We obtained from the STScI archive the WFPC2 observations in the F336W, F439W, and F814W broad band filters (which correspond to the U, B, I Johnson filters, respectively) as well as in the F658N filter which corresponds to redshifted H α . These data were cleaned for cosmic ray events and reduced following the standard procedures described in the WFPC2 data analysis tutorial. Figure 3 shows the 3σ ellipses to the spatial distribution of the X-ray source events overlaid on the U, H α and I band images. Because of the small field of view of WFPC2, 10 X-ray sources (4 of which are ULXs) are not included in this figure. Yellow ellipses correspond to sources with X-ray luminosity above 10^{39} erg s $^{-1}$, green ellipses correspond to sources with X-ray luminosities between 3×10^{38} and 10^{39} erg s $^{-1}$, and blue ellipses to sources less luminous than 3×10^{38} erg s $^{-1}$. Marked with an “X” are the 50 brightest young star-clusters (age < 30Myr) in the Antennae, from Table 1 of Whitmore et al. (1999). Marked with an “+” the 25 brightest intermediate age ($0.25\text{Gyr} < T < 1\text{Gyr}$) and diamonds the globular clusters from Tables 2 and 3 of the same work. Foreground stars are marked by circles. The ages of the clusters are based on their detection in the H α band and their optical colours, and are also obtained from Whitmore et al. (1999). Unfortunately, because of the small field of view of the WFPC2 it is not possible to identify sources common to the optical and the X-ray images, which we could use to compare their absolute astrometry. Therefore, we assume that the absolute astrometry of the WFPC2 images is good within $0.9''$ to $1.5''$ arcsecond (Biretta et al. 2000).

The properties of the optical counterparts of the 39 X-ray sources within the WFPC2 field, are listed in Table 2A, where column (1) gives the number of the X-ray source from Table 1 in Paper II, Column (2) gives its photon index and Columns (3) and (4) give Logarithm of the soft (0.1-2.5 keV) and hard band (2.5-10.0 keV) luminosities respectively, corrected for Galactic absorption, in units of erg s $^{-1}$. Column (5) gives the optical source number from Tables 1 and 2 of Whitmore et al. (1999). Column (6) gives the angular distance of the X-ray source from each optical counterpart and Columns (7)-(10) give the V band absolute magnitude, and the U-B, B-V, V-I colors respectively. Finally Column (11) gives the evolutionary state of each cluster based on the optical colors. We consider an X-ray source as coincident with an optical source if their separation is less than $2''$. This takes into account the uncertainties in the absolute astrometry of *Chandra* and HST. Optical sources which fall within the 3σ ellipse of an X-ray source, but have offsets larger than $2''$, are considered as possibly associated. We find 8 X-ray sources coincident with 18 young stellar clusters (separation smaller than $2''$) and 13 sources possibly associated with 25 young and 2 intermediate age stellar clusters. These numbers are only indicative since the list of optical clusters we used is not

complete by any means. There may well be more sources with fainter optical counterparts as is discussed later.

In order to quantitatively assess the chance coincidence probability, we created 10 source lists from the original optical source lists but with the coordinates of each source shifted by a random amount ranging between $\pm 5''$ and $\pm 25''$ in both RA and Dec. These limits were chosen in order to make sure that the new random sources will neither fall inside the positional error box of the original sources nor will fall outside the region of maximum source density in the galaxy. The latter is particularly important since the distribution of both the optical and X-ray sources is not uniform (for the same reason we cannot simply perform a calculation based on the surface density of the sources in each band). We find that 6 ± 2 X-ray sources could be associated by chance with 8 ± 4 optical sources. So the majority of the associations are likely to have a real astrophysical origin.

We searched for fainter optical counterparts using the star clusters reported in the earlier work of Whitmore & Schweizer (1995), who present the full list of star-clusters detected in an HST/WFPC observation of the Antennae down to a limiting V magnitude of ~ 23 . However, since these data were obtained with WFPC before the HST mirror refurbishing the spatial resolution and the positional accuracy of the sources is not as good as for the later WFPC2 data. We find a total of 25 X-ray sources with 177 optical counterparts from the Table 1 of Whitmore & Schweizer (1995). In Table 2B we present the properties of the secure optical counterparts (offset less than $2''$): Column (1) gives the X-ray source, Column (2) gives the optical source from Table 1 of Whitmore & Schweizer (1995), Column (3) gives the distance between the optical and the X-ray counterpart, Column (4) gives the V band magnitude of each cluster and Column (5) gives the V-I colour (also from Whitmore & Schweizer 1995). We find that, in addition to the 8 X-ray sources with secure bright optical counterparts, there are 16 X-ray sources with faint optical counterparts within a $2''$ error circle. Of the 14 ULXs in the WFPC2 field, only 10 have a secure optical counterpart, while 4 have counterparts with larger offsets ($2'' - 4''$). For the 25 less luminous X-ray sources, encompassed by the WFPC2 field, 14 have a secure optical counterpart. The other 11 may either have a fainter counterpart or a larger offset.

In Fig. 3d we show the offsets of each source from its nearest optical counterpart for the ULXs (upper left) and sources in the $3 \times 10^{38} - 10^{39}$ luminosity range (upper right). For this figure we used the source lists of Whitmore et al. (1999) as well as the more complete lists of Whitmore & Schweizer (1995). The random distribution of these offsets suggests that they are not due to a misalignment of the X-ray and optical images. From the inspection of the WFPC2 images we find that some X-ray sources have optical counterparts which are closer than those tabulated in Whitmore et al. (1999) or Whitmore & Schweizer (1995). Therefore, in order to assess the reality of the measured offsets we detected all the sources in the I-band WFPC2 image using the IRAF *daofind* task as described in Whitmore & Heyer (1995). We set a detection limit of 7σ above the local background of each chip, in order to minimize the detection of stars and spurious sources. We find a to-

tal of ~ 2000 sources over the WFPC2 field of view. The bottom panel of Fig. 3d shows the offsets between the X-ray sources and their nearest optical source from this list (ULXs left and sources in the $3 \times 10^{38} - 10^{39}$ luminosity range in the right). It is clear that the inclusion of fainter sources does not alter the fact that some X-ray sources are offset even up to $\sim 2''$ from their nearest optical source. Whitmore et al. (2002, private communication) indicated that there is an offset of $\sim 1''$ in the absolute astrometry of WFPC2. However, the random distribution of the offsets we measure, suggests that they are not due to discrepancies between the absolute astrometry of the optical and *Chandra* observations.

4.2. Radio

The Antennae galaxies have recently been observed with the VLA in the BnA, CnB and B configurations at 6cm and 4cm (Neff & Ulvestad 2000; NU2000). The beam-size was $1.72'' \times 1.52''$ for the 6cm observations and $1.36'' \times 0.96''$ for the 4cm observations. The beam area of these observations is ~ 10 times larger than that of *Chandra*. In Figure 4 we show the soft (0.3-2.0 keV) and medium (2.0-10.0 keV) band X-ray images with the radio sources marked as crosses if they have a flat radio index ($\alpha > -0.4$) and X if they have a steeper index. On the same image we have plotted the X-ray source error ellipses following the notation of Fig. 4.

From these images it is clear that there are some X-ray sources positionally associated with radio sources. Again, we consider an X-ray and radio source as coincident if their separation is smaller than $2''$, and as possibly coincident if their separation is larger but the radio source falls within the 3σ ellipse of the X-ray source. We find a total of 22 X-ray sources associated with 41 radio sources detected in either band; 16 of them have steep non-thermal radio spectra, 5 of which are ULXs. We find 6 X-ray sources with a flat thermal spectrum radio counterpart, but none of them is a ULX. It is possible that one X-ray source may coincide with more than one radio source. Table 3 presents the X-ray and radio properties of these sources: Columns (1) and (2) give the names of the X-ray and radio sources. We assign two numbers to each radio source: the first is the region number from the list of NU2000 and the second correspond to the order of the source in each region (in Table 5 of NU2000). Columns (3)-(6) give the distance from the X-ray source in arcseconds and the flux of the sources detected in the 6 cm and 4 cm bands in μJy . For the distances and the fluxes we used the data from Table 5 of NU2000 in order to have the same spatial resolution in both bands. Columns (7)-(9) give the soft (0.1-2.5 keV) and hard (2.5-10.0 keV) band luminosities, corrected for Galactic absorption, and the photon index for the X-ray sources. Finally, Columns (10) and (11) give the radio luminosity at 6 cm and the 4-6 cm radio spectral index. In the case of radio sources which belong to larger groups of sources we give the parameters of both the individual sources and the group. Usually the radio spectral index refers to the integrated emission of the group, but is dominated by the brightest sources. In order to estimate the chance coincidence probability we followed the same procedure as with the optical sources. We estimate 11 ± 3 X-ray sources to be possibly coincident by chance

with 24 ± 9 radio sources.

4.3. Infrared

The Antennae galaxies have been extensively observed in the infrared band. ISO observations (with a spatial resolution of $\sim 20''$) showed that there is a large amount of diffuse dust associated with the system (Mirabel et al. 1998, Vigroux et al. 1996). Low spatial resolution mid-IR spectroscopy with the ISO SWS and LWS showed that the IR emission of this galaxy is dominated by early type stars (Fisher et al. 1996; Kunze et al. 1996), and give a lower limit of $65M_{\odot}$ for the upper mass cutoff of the IMF. The effective temperature of the stellar populations corresponds to that of O5 type stars. The IR spectrum of the obscured overlap region is well fit with a young starburst ($\sim 7 \times 10^6 \text{ yr}$).

More recently, Mengel et al. (2001) presented near-IR imaging/spectroscopy of 5 star-clusters detected in the H α band. Four of these clusters contain X-ray sources (two of them are the nuclei) and one is in the neighborhood of an X-ray source. Stellar population synthesis modeling of these star clusters (coincident with our sources 34, 3 and 5) shows that their populations are very young (ages $\sim 3.7 - 8 \text{ Myr}$) with very large effective temperatures ($\sim 35 - 40 \text{ K}$), consistent with the ISO results. Gilbert et al. (2000) also presented NIR spectroscopy of the star-clusters associated with source 3. They also found that it is very young ($\sim 4 \text{ Myr}$) and highly obscured ($A_V = 9 - 10 \text{ mag}$). In contrast the two nuclei have much older populations (ages $\sim 65 \text{ Myr}$). Although the southern nucleus seems not to host any active star-formation (Gilbert et al. 2000; Mengel et al. 2001), the northern nucleus (NGC 4038) has both an old population ($\sim 60 \text{ Myr}$) and a concentration of young stars ($\sim 6 \text{ Myr}$) located northward of the K-band peak.

4.4. Atomic and molecular gas observations

Recently Gordon et al. (2001) observed the Antennae galaxies in the 21cm HI line with the Australia Telescope Compact Array. They find a total HI mass of $\sim 5 \times 10^9 M_{\odot}$, about half of which is concentrated in the disk. They also found large concentrations of gas in the overlap region. This large pool of gas can fuel vigorous bursts of star-formation as the merging evolves. Fig. 5 presents an VLA HI image obtained by J. Hibbard (Hibbard et al. 2001). The resolution of this image is $11.4'' \times 7.4''$. We have plotted contours in different levels of column density (using the conversion factors from Hibbard et al. 2001). Three things are clear from this image. a) The southern nucleus is situated in a large reservoir of gas, whereas the atomic hydrogen in the area of the northern nucleus is depleted. b) Most of the discrete X-ray sources are found in the outskirts of large concentrations of gas. This could be a selection effect since the column density in these regions is typically $10^{23} - 10^{24} \text{ cm}^{-2}$, enough to absorb X-rays up to 5 keV or more. c) The fact that the measured column densities from the X-ray spectra are much lower than those inferred by the HI image (typically one order of magnitude less), suggests that the detected sources lie on the surface of the galactic disks. Any sources embedded in the disks, or on their far side, cannot be observed because of obscuration.

The Antennae have also been observed in CO bands (Wilson et al. 2001). These observations showed that most of the molecular gas is in the two nuclei and 5 supergiant molecular clouds. Although, the peak associated with the northern nucleus is not positionally coincident with the HI peak in the same region, the CO peaks in the five molecular clouds are spatially coincident with the HI peaks.

5. DISCUSSION

5.1. Ultra Luminous X-ray sources: $L_X > 10^{39} \text{ erg s}^{-1}$

Because of their extreme luminosities, exceeding those expected from a neutron star or stellar mass black-hole binary, ULXs are intriguing sources found in a number of external galaxies (e.g. Fabbiano 1995; Marston et al. , 1995). If they are accretion binaries, with spherically accreting black holes, black hole masses may be in the $M \sim 10 - 1000 M_\odot$ range (e.g. Makishima et al. 2000, Ptak & Griffiths, 1999). Other suggested possibilities include beamed lower-mass binaries (King et al. 2001), and luminous SNRs exploding in dense media ($\sim 10^6 \text{ cm}^{-3}$; cSNRs) (e.g. Plewa 1995; Fabian & Terlevich 1996).

In the Antennae we detect 18 ULXs. Of these, 3 are variable, and 4 are detected with luminosities above $10^{40} \text{ erg s}^{-1}$. As discussed in Paper II, sources with $L_X > 10^{39} \text{ erg s}^{-1}$ have hard X-ray spectra with power-law indices $\Gamma \leq 2.0$. The two most luminous of them (sources 16 and 42) have extremely hard X-ray spectra with photon indices of $\Gamma \sim 1.2$. For these sources there is also evidence of gaussian emission lines (N IV triplet (0.43 keV), Mg IX triplet (1.33-1.34 keV) and Mg XIII (1.5 keV)). This result is quite surprising given the lack of any Fe-L emission around 1.0 keV and of any thermal continuum in their spectra (Paper II and §3.) and suggests either fluorescence or photoionisation of the ambient gas by the intense emission from the central X-ray source.

Although cSNR models predict hard X-ray spectra, like those observed in our sources (Plewa 1995; Franco et al. 1993), it is unlikely that they account for the majority of our brightest ULXs, since the latter do not have clear radio counterparts. Based on the lightcurve of SN1988Z which is one of the best studied examples of cSNRs (Arextaga et al. 2001), we estimate that for an X-ray luminosity of $\sim 10^{40} \text{ erg s}^{-1}$ we should detect a radio counterpart with a flux of $\sim 1 \text{ mJy}$ at 6cm, but we do not. Such a source should be detectable in the radio observations of NU2000 which have a detection limit of $\sim 50 \mu\text{Jy}$ at 6 cm. Of the lower luminosity sources ($L_X \sim 10^{39} - 10^{40} \text{ erg s}^{-1}$) only 5 have possible radio counterparts. Four of them (26, 29, 33,34), which have steep radio spectra, could still have some contribution from SNRs.

X-ray binary (XRB) counterparts are a more likely possibility: the X-ray spectra of the ULXs in the Antennae can be fit with power-laws in the range of those observed in XRB spectra (e.g., Van Paradijs 1999) and their co-added spectrum (§3.) is well fit with a composite disk-BB plus power-law model, with comparable strengths in the two components, as seen in black-hole binaries in the Very High State (VHS; e.g., Esin et al. 1997). However, at variance with VHS black hole binaries which have cooler inner disks (e.g., Tanaka & Shibazaki 1996; however see

Esin et al. 1997 for some exceptions), the inner temperature of the model accretion disk for these sources is rather large, $\sim 1.2 \text{ keV}$. Moreover, the slope of the hard component in the Antennae ULXs is much flatter ($\Gamma \sim 1.2 - 1.5$) than for most black-hole binaries in the VHS ($\Gamma \sim 2.5$; e.g., Tanaka & Lewin 1995), suggesting that if ULXs are XRBs they probably belong to a different population than the known Galactic black-hole binaries in high/very high state.

The spectral parameters of the Antennae ULXs are similar to those of Galactic microquasars (e.g., Miller et al. 2001), suggesting a possible link, but the luminosities are much larger. From the X-ray spectra of the ULXs we cannot distinguish between X-ray binaries with early type companions (High Mass X-ray Binaries; HMXBs) and X-ray binaries with late type companions (Low Mass X-ray Binaries; LMXBs), since the X-ray spectra provide information only on the nature of the accreting object. However, association with young stellar clusters suggests that their majority is related to HMXBs.

Both spectral parameters and luminosities of Antennae ULX are consistent with the properties of other ULXs, including time-variable sources with the characteristic high/soft - low/hard transitions observed in black hole binaries (e.g., Makishima et al. 2000; LaParola et al. 2001; Kubota et al. 2001). If the ULXs in the Antennae are black hole binaries, with spherical accretion onto the black hole, their extreme high X-ray luminosities suggest black hole masses in the $\gg 10\text{-}1000 M_\odot$ range. As for the other ULXs, the high temperatures we infer for the inner part of the accretion disk are inconsistent with black holes in this mass range, unless rotating black holes (e.g. Makishima et al. 2000) or slim/thick accretion disks (e.g. Watarai et al. 2000) are invoked.

An alternative model suggested for these sources, that of moderate beaming, would not require such massive black holes (King et al. 2001). Our comparison of X-ray and optical images of the Antennae (§3.1) may support this possibility at least for some sources. Although 10 out of 14 ULXs in the Antennae observed with the Hubble WFPC2 have possible optical associations (a stellar cluster down to a limiting magnitude of $m_V = 23 \text{ mag}$, within a radius of $2''$), only three can be securely associated with a stellar cluster (distance less than $1''$; Fig. 3d). The other 4 of these ULXs may have even more distant optical counterparts. The $1'' - 2''$ offsets (corresponding to a projected physical distance of $\sim 300 \text{ pc}$) between the X-ray and the stellar clusters measured for most of these sources are reminiscent of runaway binaries. Runaway binaries are the result of deviation from spherical symmetry during SN explosions (see van den Heuvel et al. 2000 for a discussion of these systems). Van Paradijs & White (1995) explain the wide Galactic latitude distributions of LMXBs with this mechanism.¹

Runaway binaries are not likely to be massive systems, as shown by the narrower distribution of the Galactic latitude of LMXBs with black holes compared to those with neutron star accretors (White & van Paradijs, 1996), and by SNe models for massive stars (Arnett, 1996), where only a small fraction of the stellar mass is expelled dur-

¹ However, the galactic black-hole candidate XTE J1118+480 is located in the halo of the Galaxy. It is unclear whether this source was formed in the Galactic plane and the kicked out, or was formed in the halo.

ing the explosion, resulting in very small, if any, kicks to the remnants. The possibility that some at least of the ULXs may be runaway binaries is supported by the similar offsets measured in less luminous sources (right panels in Fig. 3d), which are likely to be normal lower-mass binaries and would be subject to kicks, by analogy with the galactic XRB observations.

The implications of these offsets will be discussed further in Paper IV (Zezas & Fabbiano 2002), together with constraints to ULX models derived from the luminosity distribution of the Antennae sources.

5.2. Sources with $L_X \sim 10^{38} - 10^{39} \text{ erg s}^{-1}$

X-ray spectra of these sources are much less constrained than those of the more luminous sources, with spectral parameters covering a very wide range of values ($1.7 < \Gamma < 7$, and N_H ranging from the galactic value up to $\sim 3 \times 10^{22} \text{ cm}^{-2}$; Paper II). The co-added spectrum of the sources with $L_X > 3 \times 10^{38} \text{ erg s}^{-1}$, which is the Eddington limit for a neutron star, is best fit with a power-law ($\Gamma = 2.0$) plus two thermal plasma models ($kT=0.76 \text{ keV}$ and 0.28 keV). The parameters of the thermal component are reminiscent of those obtained for the superwinds in the nearby galaxies M 82 and NGC 253 (Strickland et al. 1999, 2000; Moran et al. 1999), suggesting that a fraction of the total emission of these sources is produced by a multicomponent thermal plasma. The value of the photon index is steeper than that of the higher luminosity sources and is at the borderline between that observed for black-hole binaries in high state and magnetized neutron star binaries in the Galaxy (e.g. van Paradijs, 1999). However, the co-added spectrum can be fitted equally well with a harder power-law in the range of neutron star binaries ($\Gamma = 1.5$), a multi-temperature disk-BB ($kT=0.24$) and a thermal plasma ($kT=0.66$). This disk-BB temperature component is much lower than that of the ULXs and is consistent with that observed in VHS Galactic black-hole binaries (e.g. Tanaka & Shibazaki, 1996; Makishima et al. 2000). The best fit power-law slope, instead, is flatter than that of Galactic black-hole binaries.

Of the 18 sources in this luminosity range only 10 are securely associated with a stellar cluster of a limiting magnitude $m_V = 23 \text{ mag}$. The V-I colours of these clusters are consistent with ages less than 100 Myr, as determined from evolutionary synthesis models (Leitherer et al. 1999). Ten of these sources are associated with steep spectrum radio sources. Thus these sources are closely connected with the younger stellar population.

The lowest luminosity sources (i.e., those with luminosities below the Eddington limit for a neutron star binary, $L_X \sim 3 \times 10^{38} \text{ erg s}^{-1}$), are most probably a mixture of SNRs and neutron star binaries. This is suggested by the steepness of their X-ray spectra, which have a mean photon index of 2.5 as measured from their co-added spectrum. Fits to the same spectrum also require a thermal component with a temperature of 0.18 keV, most probably associated with diffuse gas in the neighborhood of the sources. This component becomes more important in the lowest luminosity sources since it is not negligible compared to the source’s emission. We note that models with a multi-temperature disk-black body spectrum do not give acceptable fits, suggesting that black hole binaries in high

state are not the dominant population in this luminosity range. This is expected since black hole binaries in high state emit close to their Eddington luminosity which is higher than $\sim 3 \times 10^{38} \text{ erg s}^{-1}$. Also it is unlikely that these sources are black-hole binaries in the low state, since in this case their luminosity would be less than 10% of their Eddington luminosity (e.g. Nowak 1995). Indeed the slope of the power-law component is steeper than the typical slopes of black-hole binaries in low state ($\Gamma \sim 1.5 - 1.7$; e.g. Esin et al. 1997).

The sources with soft X-ray spectra ($\Gamma > 3$) could well be supernova remnants, and this explains the excess of softer sources found at lower luminosities. Indeed, some of them have radio counterparts with steep radio spectral indices. NU2000 estimate that about 50 SNRs are enough to produce the observed radio emission for most non thermal radio sources, consistent with the number of SNRs required to explain the observed X-ray luminosity of their counterparts.

Whitmore et al. (1999) identified some of the sources detected with the HST/WFPC2 as globular clusters. None of these sources are found to be associated with an X-ray source. This could be due to our relatively high detection threshold, since the dominant X-ray population in globular clusters is LMXBs which have luminosities close to or lower than our detection limit of $10^{38} \text{ erg s}^{-1}$.

5.3. Highly obscured sources

As shown in Paper II, six sources have column densities ranging from $0.35 \times 10^{22} \text{ cm}^{-2}$ up to $3.4 \times 10^{22} \text{ cm}^{-2}$, i.e. $\sim 10 - 100$ times the Galactic N_H along the line of sight. These sources (12, 24, 25, 34, 35 and 36), are found predominantly in the impact region between the two galaxies and in the neighborhood of molecular clouds (§3) (see Fig. 5). Although the majority of these sources have low count rates, their intrinsic luminosities can be high because of their very large N_H . The most extreme examples are Sources 35 and 24 with an absorption corrected luminosity of $8 \times 10^{39} \text{ erg s}^{-1}$ and $3 \times 10^{41} \text{ erg s}^{-1}$ respectively. It is unlikely that both sources are background QSOs seen through the dense gaseous disk of the Antennae system, because the N_H inferred for the X-ray fits are well below those measured from observations at 21cm ($4.2 \times 10^{24} \text{ cm}^{-2}$ and $\sim 6.0 \times 10^{24} \text{ cm}^{-2}$ for Source 35 and Source 24 respectively; Gordon et al. 2001). This comparison suggests that both sources are situated within the molecular clouds, and reside in young stellar clusters, a conclusion supported by the fact that both sources are coincident with strong non-thermal radio sources. Based on the conservative model of Condon & Yin (1990) NU2000 estimate a SN rate of 5.1 SNe per 10^3 yr for Source 35, which is the strongest non-thermal radio source in the Antennae. Less conservative estimates give 10 times higher rates. Observations of other star-forming galaxies (eg M82, Zezas et al. 2001; NGC3628, Strickland et al. 2001), reinforce the conclusion that X-ray sources with luminosities up to $10^{41} \text{ erg s}^{-1}$ are not uncommon in very active star-forming regions. Therefore, these sources could be either extreme cases of ULXs or complexes of luminous X-ray binaries in compact star-forming region.

5.4. The northern nucleus: NGC 4038

Based on the radio coordinates of the Northern nucleus we identify it as our source 25. The offsets of the centroid of this source (0.3-10.0 keV band) from the 4 cm and 6 cm radio sources are $1.1''$ and $1.87''$, respectively. In this region there are three more sources (sources 24, 22, 26), of which the last two are only detected above 2.0 keV. This is not surprising, given the large amounts of molecular gas present in this region (Wilson et al. 2000). The luminosity of the nucleus is modest ($\sim 10^{39}$ erg s $^{-1}$) just slightly higher than the luminosity of two of the neighboring sources. Its spectrum is very soft ($\Gamma = 8.26^{+1.74}_{-2.61}$) with a relatively large absorbing column density ($N_H = 1.07^{+0.36}_{-0.42} \times 10^{22}$ cm $^{-2}$). The two nearby sources have similar X-ray spectra. The steep spectrum of the nuclear sources suggests thermal emission. The fit with a PO+RS model results in a temperature of $kT \sim 0.8$ keV (Table 7 of Paper II), which could be consistent with thermal emission by a supernova driven superwind (e.g., Heckman et al. 1980; Strickland et al. 2000). This interpretation is supported by the relatively flat radio spectral index of the nucleus ($\alpha = -0.58 \pm 0.20$) and the presence of a number of young star-clusters in the area. A more detailed discussion on this will be presented in Paper V (Fabbiano et al. in preparation).

5.5. The southern nucleus: NGC 4039

We identify the southern nucleus as our source 29 based on its radio position. It has an X-ray luminosity of 7.7×10^{39} erg s $^{-1}$ and a steep photon index of $3.3^{+0.5}_{-0.4}$. The inclusion of a thermal component improves the fit and gives a relatively absorbed power-law ($N_H \sim 0.14 \times 10^{22}$ cm $^{-2}$) with a steep slope ($\Gamma \sim 2.14$). The temperature of the thermal component is 0.77 keV. The existence of the additional thermal component is consistent with the fact that an extended component is associated with this source. These results suggest that there is a population of X-ray binaries together with diffuse gas, possibly from an outflow from an earlier starburst. Indeed, IR spectroscopic results show that the nucleus of NGC 4039 does not host any recent star-formation but it has an old stellar population with an age of ~ 60 Myr (Mengel et al. 2001). At this age the majority of the OB type stars have formed supernovae and most of the intermediate type stars are evolving off the main sequence. However, it is still too early for the onset of Roche lobe overflow in late type stars, which initiates the X-ray emitting phase of LMXBs (eg. Meurs & Van den Heuvel 1989). Therefore we expect the majority of the X-ray binaries to be HMXBs (neglecting any underlying LMXBs from the bulge of NGC 4039). This is a reasonable approximation since the stellar populations are now dominated by the most recent star-formation events. The nucleus of NGC 4039 has a very steep radio spectrum suggesting that its radio emission is non-thermal, arising from SNRs, in accordance with an intermediate age starburst. These SNe may be responsible for heating the ISM in the nuclear region to X-ray emitting temperatures, consistent with the soft thermal component measured in its spectrum.

6. CONCLUSIONS

In this paper we have discussed the X-ray properties and the nature of the luminous X-ray sources discovered

with *Chandra* in the Antennae (Paper I), and analyzed in detail in Paper II, by studying the average properties of the X-ray spectra in three luminosity ranges, and by investigating the multi-wavelength environment of the X-ray sources. Our results are summarized below:

1) As reported in Paper II, 49 sources were detected with *Chandra* in the Antennae, down to a limiting luminosity of 10^{38} ergs s $^{-1}$ ($H_o = 50$); 18 of these sources are ULXs with $L_X > 10^{39}$ ergs s $^{-1}$. At least 4 of these sources are variable either with the *Chandra* observations, or in comparison with the previous *ROSAT HRI* observation (Fabbiano et al. 1997). The most luminous ULXs have very hard spectra, that can be fitted with power-laws of $\Gamma \sim 1.2$, and there is evidence of a luminosity-spectral trend, with sources becoming softer at the lower luminosities.

2) We co-added the X-ray spectra of sources in 3 luminosity ranges: $L_X > 10^{39}$ ergs s $^{-1}$ (ULXs), $3 \times 10^{38} < L_X < 10^{39}$ ergs s $^{-1}$, and $L_X < 3 \times 10^{38}$ ergs s $^{-1}$, and fitted the co-added spectra with a number of emission models. Single-component models are inadequate to fit the data in all cases.

The spectrum of sources with $L_X < 3 \times 10^{38}$ ergs s $^{-1}$ is well fitted with a composite Power-law ($\Gamma \sim 4$) and thermal Raymond-Smith ($kT \sim 0.4$ keV) model, with the thermal component accounting for 34% of the emission at energies below 2.5 keV. A good fraction of this component is likely to arise from hot ISM in the beam.

Sources with $L_X > 3 \times 10^{38}$ ergs s $^{-1}$ require three-component models, either a power-law with two Raymond-Smith components, or a powerlaw + Raymond-Smith + disk-BB. The latter model (multi-color disk black body) has been used to approximate the emission of an accretion disk in X-ray binaries (e.g. see Makishima et al. 2000).

In sources with $3 \times 10^{38} < L_X < 10^{39}$ ergs s $^{-1}$, the Raymond-Smith component accounts for a sizeable amount of the soft emission. Again, it is possible that this may be due at least in part to hot ISM in the beam. If we adopt the power-law plus two thermal components model, we obtain power-law $\Gamma \sim 2$, consistent with either black-hole binaries or magnetized neutron star binaries. The temperatures of the thermal components (~ 0.8 and ~ 0.3 keV), are in the range of those measured in the hot ISM and superwinds of nearby starburst galaxies (e.g. Strickland et al 1999). If we adopt the powerlaw + Raymond-Smith + disk-BB model, the power-law is flatter, $\Gamma \sim 1.5$, the plasma temperature is still in the range expected for a hot ISM, and the inner accretion disk temperature is in the range of those seen in Very High State Galactic black-hole binaries ($kT \sim 0.2$ keV; e.g. Tanaka & Shibazaki 1996).

In the ULX spectrum, the Raymond-Smith contribution to the emission is small. Adopting the powerlaw + Raymond-Smith + disk-BB model, the best-fit parameters are consistent with those of other ULXs (e.g. Makishima et al. 2000, LaParola et al 2001; Kubota et al. 2001). In particular the inner accretion disk temperature is large (1.13 keV), requiring a rotating massive black hole, if the accreting black hole binary picture of Makishima et al. (2000) applies.

3) Twenty three sources are found to be coincident with one or more young stellar clusters (ages < 30 Myr) and one

with an intermediate age cluster. This suggests that they are most probably associated with a young stellar population. This is also supported by the IR spectra of the four clusters with available IR spectroscopy. Comparison with *HST* data (Witmore et al 1995, 1997) shows that the majority of sources have an associated optical cluster within a 2" radius. However, there are random orientation offsets between X-ray source and optical cluster position in a number of cases, including ULXs. This suggests that, if the X-ray source originated in the star cluster, it was ejected at a certain point in its evolution, i.e. it is a runaway binary. If ULXs are runaway binaries, it is unlikely that they may be very massive. This results therefore challenges the association of ULXs with 10-1000 M_{\odot} black holes, while is in keeping with the moderate beaming model of King et al. (2001).

4) Comparison with the Neff & Ulvestad (2000) radio continuum survey of the Antennae, shows that twenty two X-ray sources have one or more radio counterparts. The majority of these have steep radio indices suggesting that SNRs are responsible at least for part of their soft X-ray emission. While fainter sources may be associated with SNRs, the ULXs are not likely to be, reinforcing the binary model for these sources. In particular, the lack of radio counterparts for the 3 most luminous X-ray sources ($L_X > 10^{40}$ erg s $^{-1}$) strongly indicates that they are not associated with young compact SNRs.

5) We find 6 sources with obscuring column densities more than 10 times higher than the Galactic along the line of sight. These sources are spatially coincident with dense molecular clouds suggesting that they are regions of in-

tense star-formation embedded in these clouds.

6) Finally, both nuclei were detected. The northern nucleus has $L_X \sim 10^{39}$ ergs s $^{-1}$, the southern nucleus is associated with extended emission and has $L_X \sim 8 \times 10^{39}$ ergs s $^{-1}$. The northern nucleus has a very soft spectrum, suggesting thermal emission, possibly related to hot winds escaping the star forming region. The southern nucleus has a composite spectrum, consisting of a thermal component plus a power-law with $\Gamma \sim 2$. This spectrum suggests both hot ISM and a contribution with X-ray binaries, which would be expected to be found in this post-starburst nucleus (age of ~ 60 Mys; Mengel et al. 2001).

These results clearly need to be followed up by more detailed deep observations of the Antennae with *Chandra*, so that individual sources can be studied with adequate statistics, instead of relying only on average properties. A ‘large’ *Chandra* observing program to pursue these objectives was approved in AO-3, and the data are beginning to be acquired.

We thank the CXC DS and SDS teams for their efforts in reducing the data and developing the software used for the reduction (SDP) and analysis (CIAO). We thank Martin Ward, Jeff McClintock, Andrea Prestwich and Phil Kaaret for useful discussions on these results. We also thank J. Hibbard for providing the HI VLA data for the Antennae. The HST data presented in this paper were obtained from the Multimission Archive at the Space Telescope Science Institute (MAST). This work was supported by NASA contract NAS 8-39073 (CXC) and NAS8-38248 (HRC).

REFERENCES

- Aretxaga, I., Terlevich, E., Terlevich, R. J., Cotter, G., & Díaz, Ángeles I. 2001, MNRAS, 325, 636
- Arnett D., 1996, *Supernovae and nucleosynthesis*, Princeton University Press
- Biretta, J. et al. 2000, WFC2 Instrument Handbook, Version 5.0 (Baltimore, STScI)
- Condon, J. J. & Yin, Q. F. 1990, ApJ, 357, 97
- Esin, A. A., McClintock, J. E., & Narayan, R. 1997, ApJ, 489, 865
- Fabian A., & Terlevich R., 1996 MNRAS, 280, 5
- Fabbiano, G. 1989, Ann. Rev. Ast. Ap., 27, 87
- Fabbiano, G. 1995, in X-ray Binaries, ed. W. H. G. Lewin, J. van Paradijs, & E. P. J. van den Heuvel (Cambridge: University Press), p. 390
- Fabbiano, G., Schweizer, F., & Mackie, G. 1997, ApJ, 478, 542
- Fabbiano, G., Zezas, A., & Murray, S. 2001, ApJ, 554, 1035 (Paper I)
- Fischer, J. et al., 1996, A&A, 315, 97
- Franco, J., Miller, W., Cox, D., Terlevich, R., Rozyczka, M., & Tenorio-Tagle, G. 1993, Revista Mexicana de Astronomia y Astrofisica, vol. 27, 133
- Georgakakis A., Hopkins A. M., Caulton A., Wiklind T., Terlevich A. I. & Forbes D. A., 2001, astro-ph/0105435
- Gilbert, A. M. et al. 2000, ApJ, 533, L57
- Gordon, S., Koribalski, B., & Jones, K. 2001, MNRAS, 326, 578
- Hibbard, J. E., Van der Hulst, J. M., Barnes J. E., Rich R. M., 2001, astro-ph/0110581
- King, A. R., Davies, M. B., Ward, M. J., Fabbiano, G., & Elvis, M. 2001, ApJ, 552, L109
- Kubota, A., Mizuno, T., Makishima, K., Fukazawa, Y., Kotoku, J., Ohnishi, T., & Tashiro, M. 2001, ApJ, 547, L119
- Kunze, D. et al. 1996, A&A, 315, L101
- Leitherer, C. et al. 1999, ApJS, 123, 3
- Makishima, K. et al. 2000, ApJ, 535, 632
- Meurs, E. J. A. & van den Heuvel, E. P. J. 1989, A&A, 226, 88
- Mengel, S., Lehnert, M. D., Thatte, N., Tacconi-Garman, L. E., & Genzel, R. 2001, ApJ, 550, 280
- Mihos, J. C. & Hernquist, L. 1996, ApJ, 464, 641
- Miller, J. M., Fox, D. W., Di Matteo, T., Wijnands, R., Belloni, T., Pooley, D., Kouveliotou, C., & Lewin, W. H. G. 2001, ApJ, 546, 1055
- Mirabel, I. F. et al. 1998, A&A, 333, L1
- Moran, E. C., Lehnert, M. D., & Helfand, D. J. 1999, ApJ, 526, 649
- Nagase, F. 1989, PASJ, 41, 1
- Neff, S. G. & Ulvestad, J. S. 2000, AJ, 120, 670
- Nowak, M. A. 1995, PASP, 107, 1207
- Plewa T., 1995, MNRAS, 275, 143
- Ptak, A. & Griffiths, R. 1999, ApJ, 517, L85
- Roberts T., & Warwick R., 2000, MNRAS, 315, 98
- Schlegel E., 1995, Reports of Progress in Physics, 58, 1375
- Strickland, D. K., Ponman, T. J., & Stevens, I. R. 1997, A&A, 320, 378
- Strickland, D. K., Heckman, T. M., Weaver, K. A., & Dahlem, M. 2000, AJ, 120, 2965
- Strickland, D. K. & Stevens, I. R. 2000, MNRAS, 314, 511
- Strickland, D.K., Colbert, E.J.M., Heckman, T.M., Weaver, K.A., Dahlem, M., Stevens, I.R., 2001, astro-ph/0107115
- Tanaka, F. & Lewin W. 1995, in X-ray Binaries, ed. W. H. G. Lewin, J. van Paradijs, & E. P. J. van den Heuvel (Cambridge: University Press), p. 126
- Tanaka, Y. & Shibazaki, N. 1996, ARA&A, 34, 607
- Terlevich, R. 1994, in Circumstellar Media in the Late Stages of Stellar Evolution, ed. R.E.S. Clegg, I.R. Stevens, W.P.S Meikle, J. van Paradijs, (Cambridge: University Press), p. 153
- Toomre, A. & Toomre, J. 1972, ApJ, 178, 623
- Van den Heuvel, E. P. J., Portegies Zwart, S. F. B. D., & Kaper, L. 2000, A&A, 364, 563
- Van Paradijs, J., 1999, in the Many Faces of Neutron Stars, ed. R. Buocheri, J. van Paradijs, M.A. Alpar (Kluwer Academic Publishers), p. 279 (astro-ph/9802177)
- Van Paradijs, J. & White, N. 1995, ApJ, 447, L33
- Van Speybroeck, L., Jerius D., Edgar, R. J., Gaetz, T. J., Zhao, P. & Reid, P. B. 1997, Proc. SPIE 3113, 89
- Vigroux, L. et al. 1996, A&A, 315, L93
- Watarai, K., Fukue, J., Takeuchi, M., & Mineshige, S. 2000, PASJ, 52, 133

- Watson M. G., 1990, in *Windows in Galaxies*, eds, Fabbiano G., Gallagher J.S., and Renzini A.
- Weisskopf, M., Tananbaum, H., Van Speybroeck, L. & O'Dell, S. 2000, *Proc. SPIE* 4012 (astro-ph 0004127)
- White, N. E. & van Paradijs, J. 1996, *ApJ*, 473, L25
- Whitmore & Heyer, 1995, http://www.stsci.edu/instrument-news/isr/wfpc2/9504/9504_1.html
- Whitmore, B. C. & Schweizer, F. 1995, *AJ*, 109, 960
- Whitmore, B. C., Zhang, Q., Leitherer, C., Fall, S. M., Schweizer, F., & Miller, B. W. 1999, *AJ*, 118, 1551
- Wilson, C. D., Scoville, N., Madden, S. C., & Charmandaris, V. 2000, *ApJ*, 542, 120
- Zezas, A., Georgantopoulos, I. & Ward, M., 1999, *MNRAS*, 308, 302
- Zezas A., Fabbiano G., Prestwich A., Ward M., & Murray S., 2001, *Procs of The Central Kiloparsec of Starbursts and AGN: The La Palma Connection*, ASP Conf Series, Vol. 249, 425, Eds. J.H. Knapen, J.E. Beckman, I. Shlosman, and T.J. Mahoney (astro-ph/0109302)
- Zezas, A. & Fabbiano G., 2002, submitted to *ApJ*(Paper IV)
- Zezas, A. & Fabbiano G., Rots A.H. & Murray S.S., 2002, submitted to *ApJ*(Paper III)
- Zhang, Q., Fall, S. M., & Whitmore, B. C. 2001, *ApJ*, 561, 727

TABLE 1A
SPECTRAL FITS OF COADDED SPECTRA

L _X range	PO		PO+RS		PO + disk bb		PO + RS + disk bb		PO + RS + RS	
	Γ	N _H ¹ χ ²	Γ N _H ¹	kT ² χ ²	Γ N _H ¹	kT _{in} ² χ ²	Γ kT _{in} ²	kT ² N _H ¹ χ ²	Γ kT ²	kT ² N _H ¹ χ ²
(1)	(2)	(3)	(4)	(5)	(6)	(7)	(8)	(9)	(10)	(11)
< 3 × 10 ³⁸	3.36 ^{+0.66} _{-0.28}	0.28 ^{+0.1} _{-0.05}	2.5 ^{+0.57} _{-0.31}	0.36 ^{+0.12} _{-0.09}	3.76 ^{+0.56} _{-0.46}	0.068 ^{+0.012} _{-0.002}				
		55.9 (22)	0.18 ^{+0.11} _{-0.07}	16.6 (19)	1.105 ^{+0.14} _{-0.06}	31.9 (20)				
3 × 10 ³⁸ – 10 ³⁹	3.37 ^{+0.32} _{-0.26}	0.23 ^{+0.052} _{-0.034}	2.25 ^{+0.22} _{-0.18}	0.66 ^{+0.04} _{-0.05}	1.8 ^{+0.28} _{-0.26}	0.15 ^{+0.03} _{-0.02}	1.54 ^{+0.41} _{-0.26}	0.66 ^{+0.06} _{-0.05}	2.02 ^{+0.24} _{-0.18}	0.76 ^{+0.07} _{-0.07}
		256.7 (85)	0.08 ^{+0.02} _{-0.02}	124.1 (83)	0.32 ^{+0.11} _{-0.06}	160.3 (83)	0.24 ^{+0.05} _{-0.06}	0.09 ^{+0.06} _{-0.03}	0.28 ^{+0.06} _{-0.03}	0.072 ^{+0.03} _{-0.02}
> 10 ³⁹	1.57 ^{+0.05} _{-0.04}	0.09 ^{+0.04} _{-0.01}	1.47 ^{+0.04} _{-0.04}	0.82 ^{+0.15} _{-0.06}	1.34 ^{+0.18} _{-0.19}	0.60 ^{+0.27} _{-0.2}	1.23 ^{+0.23} _{-0.27}	107.2 (81)	1.55 ^{+0.06} _{-0.06}	99.7 (81)
		281.4 (244)	0.078 ^{+0.008} _{-0.01}	247.6 (242)	0.066 ^{+0.022} _{-0.018}	276.0 (242)	1.13 ^{+0.47} _{-0.24}	0.81 ^{+0.05} _{-0.08}	0.042 ^{+0.019} _{-0.017}	0.77 ^{+0.07} _{-0.09}
								229.7 (240)	0.054 ^{+0.047} _{-0.012}	0.12 ^{+0.02} _{-0.03}
										232.5 (240)

¹ Absorbing column density in units of 10²² cm⁻².

² Temperature in units of keV.

TABLE 1B
INTENSITY OF THE BEST FIT COMPONENTS IN THE COADDED SPECTRA

L _X range (1)	Model Component (2)	Intensity ¹	
		(0.1-2.5) keV (3)	(2.5-10.0) keV (4)
< 3 × 10 ³⁸	PO	0.66	0.999
	RS	0.34	0.001
3 × 10 ³⁸ – 10 ³⁹	PO	0.63	0.98
	RS (high kT)	0.27	0.01
	RS (low kT)	0.1	0.01
	PO	0.47	0.99
	disk-BB	0.07	0.005
	Ray	0.46	0.005
> 10 ³⁹	PO	0.55	0.823
	disk-BB	0.38	0.175
	Ray	0.07	0.002
	PO	0.91	0.999
	RS (high kT)	0.06	0.001
	RS (low kT)	0.03	0.0

¹ Relative contribution of each component in the total emission in each band.

TABLE 2A
SOURCES WITH BRIGHT OPTICAL COUNTERPARTS

X-ray Source No (1)	Γ (2)	Log(L _x)		Optical Source No (5)	Dist. (arcsec) (6)	M _v (7)	U-B (8)	B-V (9)	V-I (10)	Notes (11)
		soft (3)	hard (4)							
5	7.22 ^{+2.39} _{-1.71}	39.02	37.46	40	2.3	-11.46	-0.7	0.06	0.17	young
5				46	2.6	-11.37	-0.79	-0.19	-0.15	young
6	4.95 ^{+3.64} _{-1.51}	38.78	37.45	12	0.7	-12.32	-0.71	0.0	0.12	young
6				47	0.8	-11.37	-0.68	0.05	0.12	young
6				50	0.6	-11.33	-0.8	-0.05	0.22	young
7				22	2.4	-11.78	-0.69	0.04	0.27	young
10	> 5.94	38.75	37.06	1	2.0	-13.92	-0.61	0.02	0.49	young
10				44	2.4	-11.38	-0.31	0.58	1.15	young
11	1.54 ^{+0.19} _{-0.18}	39.47	39.81	49	1.5	-11.34	-0.56	0.28	0.32	young
13	4.19 ^{+1.84} _{-1.22}	37.24	38.66	7	2.3	-9.83	0.1	0.27	0.51	interm
15		38.40 ¹		25	0.3	-11.75	-0.7	0.26	0.42	young
15				23	3.3	-11.78	-0.71	0.09	0.19	young
22		38.38	38.18	3	2.1	-13.68	-0.72	0.06	0.06	young
24	5.73 ^{+2.16} _{-1.35}	38.88	37.77	38	2.0	-11.5	-0.07	0.82	1.0	young
24				34	2.2	-11.61	-0.24	0.64	0.84	young
25	8.26 ^{+1.74} _{-2.61}	38.63	37.35	3	1.4	-13.68	-0.72	0.06	0.06	young
25				4	1.9	-12.9	-0.67	0.05	0.07	young
30				13	2.4	-9.41	0.99	1.42	2.04	interm
34	6.48 ^{+0.62} _{-3.52}	39.06	38.15	39	0.59	-11.48	-0.68	0.15	0.24	young
34				30	0.6	-11.67	-0.69	0.14	0.14	young
34				33	0.9	-11.63	-0.67	0.17	0.09	young
34				26	1.0	-11.75	-0.55	0.31	0.73	young
34				14	1.3	-12.2	-0.79	0.37	0.28	young
34				9	1.3	-12.38	-0.73	0.39	0.34	young
34				20	1.5	-11.95	-0.65	0.53	0.46	young
34				11	1.6	-12.34	-0.28	0.84	0.67	young
36	> 3.71	38.0 ¹		18	1.4	-12.03	-0.67	0.25	0.31	young

¹ The luminosity for these sources is in the 0.1-10.0 keV band (from Table 1).

TABLE 2B
OPTICAL PROPERTIES OF THE SOURCES WITH FAINT OPTICAL COUNTERPARTS

X-ray Source (1)	Optical Source (2)	Dist. (arcsec) (3)	Vmag (4)	V-I (5)	X-ray Source (6)	Optical Source (7)	Dist. (arcsec) (8)	Vmag (9)	V-I (10)
5	347	0.6	21.12	-0.04	25	414	1.1	21.84	1.03
5	345	0.9	20.34	0.44	25	442	1.4	17.46	0
5	352	1.6	21.88		25	411	1.4	21.57	0.29
5	377	2.0	22.31	1.6	25	412	1.8	21.5	0.25
5	329	2.0	21.59		25	403	1.9	21.93	0.74
6	479	0.2	20.05	-0.16	25	450	1.9	18.25	0.05
6	483	0.7	21.39		29	40	1.3	22.41	
6	485	0.7	18.72	0.21	29	49bc	2.0	17.71	1.57
6	481	0.8	19.47	0.06	31	494	1.4	21.69	0.08
6	487	0.9	21.36	0.54	31	498	1.6	19.85	0.28
6	491	1.9	20.56	0.46	33	65	0.7	21.94	0.33
7	296	1.3	22.43	0.86	33	55	1.8	22.73	
7	297	1.4	19.54	0.29	34	87	0.6	19.52	0.65
7	292	1.8	20.17	0.67	34	86	0.7	20.17	0.55
7	284	1.9	19.96	0.36	34	90	1.1	18.59	0.59
10	573	0.9	22.1	1.02	34	88	1.1	19.36	0.87
10	581	1.0	22.23		34	89	1.3	18.52	0.92
10	571	1.5	20.53	0.74	34	75	1.6	20.8	0.76
10	580	1.8	23.2		34	77	1.6	21.8	
10	562	2.0	21.83	0.23	35	109	0.4	22.77	
11	244	0.7	21.77	0.53	35	105	1.5	22.47	
11	235	1.0	20.94	0.29	36	359	1.1	22.74	1.89
11	253	1.6	19.73	0.52	36	384	1.2	21.29	
15	233	0.7	21.79		36	389	1.4	19.27	0.39
15	229	0.7	20.18	0.83	36	392	1.8	20.29	1.02
15	236	0.8	19.07	0.24	36	382	2.0	21.99	0.65
15	218	1.2	21.57	0.47	37	38	1.7	20.59	1.48
15	243	1.3	20.89	0.35	39	124a	1.3	22.94	19.68
15	230	1.3	21.85		40	114	0.3	22.29	0.82
15	217	1.5	22.44	1.2	40	116	1.4	22.3	0.51
15	226	1.9	20.17	0.29	41	161	1.1	21.52	1.38
16	698	1.7	21.89	0.35	42	362	0.3	20.44	0.44
16	695	1.7	22.1	0.68	42	370	0.7	21.69	0.83
17	556	1.8	22.51	1.11	42	374	0.9	23.05	
19	36	2.0	21.59	0.87	42	348	1.4	21.65	0.79
20	717	1.4	21.84	0.27	42	368	1.6	22.03	
20	720	1.7	22.17	0.46					
22	412	0.9	21.5	0.25					
24	493	0.4	19.99	0.39					
24	489	0.5	20.3	1.19					
24	492	1.0	20.79	1.61					
24	480	1.3	20.54						
24	500	1.5	21.3						
24	501	1.8	20.21	1.72					

TABLE 3
RADIO PROPERTIES OF THE SOURCES

Source		6 cm		4 cm		X-ray	Lumin.	Γ	Log(L_{radio})	Radio index
X-ray	Rad.	Dist. (arcsec)	Flux (μJy)	Dist. (arcsec)	Flux (μJy)	Soft	Hard		(erg/s/Hz)	
(1)	(2)	(3)	(4)	(5)	(6)	(7)	(8)	(9)	(10)	(11)
5	11-2	2.1	90 \pm 19	2.6	64 \pm 10	39.02	37.46	7.22	25.96	
5	11-3	2.8	355 \pm 29	2.5	147 \pm 10				26.55	
5	11-Total		445 \pm 35		290 \pm 17				26.65	-0.77 ± 0.22
6	12-1	2.3	55 \pm 11	1.5	70 \pm 10	38.78	37.45	4.95	25.74	
6	12-2	1.0	80 \pm 11	0.5	41 \pm 10				25.91	
6	12-Total		135 \pm 16		111 \pm 14				26.13	-0.35 ± 0.34
7	10-1	2.0	48 \pm 11	2.6	56 \pm 10	38.5 ¹			25.68	
7	10-2	2.7	217 \pm 30	2.5	75 \pm 10				26.34	
7	10-Total		265 \pm 32		131 \pm 14				26.43	-1.27 ± 0.32
10	13-4	1.9	47 \pm 11			38.75	37.06	> 7.6	25.67	< -0.81 ± 0.74
10	13-5	1.8	62 \pm 11						25.79	< -1.30 ± 0.68
13	8-1	2.5	48 \pm 11			37.24	38.66	4.19	25.68	< -0.84 ± 0.73
15	8-2	0.9	113 \pm 11	0.99	90 \pm 10	38.40 ¹		4.41	26.06	-0.41 ± 0.29
15	8-3	2.6	72 \pm 11						25.86	< -1.57 ± 0.66
17	7-13	2.1	48 \pm 11			38.12 ¹			25.68	< -0.84 ± 0.73
22	7-2	2.3	145 \pm 11	2.1	174 \pm 10	38.38	38.18	2.44	26.15	
22	7-3	1.0	96 \pm 11						25.98	
22	7-Total		241 \pm 16		174 \pm 10				26.38	-0.58 ± 0.2
23	1A-2	2.8	44 \pm 11			38.25 ¹			25.64	-0.69 ± 0.75
24	7-10	1.0	1354 \pm 23	0.9	659 \pm 10	38.88	37.77	5.73	27.13	
24	7-11			1.5	275 \pm 10					
24	7-12			2.8	104 \pm 10					
24	7-Total		1354 \pm 23		1038 \pm 18				27.13	-0.48 ± 0.13
25	7-2	1.1	145 \pm 11	1.87	174 \pm 10	38.63	37.35	8.26	26.16	
25	7-3	1.2	96 \pm 11						25.98	
25	7-Total		241 \pm 16		174 \pm 10				26.38	-0.58 ± 0.2
25	7-7	2.9	204 \pm 11	2.8	153 \pm 10				26.31	-0.52 ± 0.2
26	7-7	1.7	204 \pm 11	1.5	153 \pm 10	39.02 ¹		1.34	26.31	-0.52 ± 0.2
26	7-8	2.0	109 \pm 11	2.2	77 \pm 10				26.04	-0.62 ± 0.32
29	1-2	0.7	513 \pm 11	0.8	295 \pm 10	39.53	39.19	3.33	26.71	
29	1-3	2.1	226 \pm 11	2.0	224 \pm 10				26.36	
29	1-Total		739 \pm 16		519 \pm 14				26.87	-0.63 ± 0.14
29	1-5	3.7	365 \pm 21	3.9	327 \pm 25				26.56	-0.2 ± 0.21
33	2-2	1.4	241 \pm 31	1.8	180 \pm 28	38.78	38.54	3.33	26.38	-0.52 ± 0.38
34	2-2	2.2	21 \pm 31	1.9	180 \pm 28	39.06	38.15	6.48	25.39	-0.52 ± 0.38
34	2-6	0.4	2257 \pm 20	0.4	1957 \pm 21				27.36	
34	2-7	2.2	59 \pm 11						25.77	
34	2-Total		2316 \pm 20		1957 \pm 21				27.37	-0.3 ± 0.13
34	2-8	4.7	49 \pm 11	3.5	41 \pm 10				25.69	-0.32 ± 0.61
35	3-5	1.3	1121 \pm 19	1.3	930 \pm 22	38.33	39.63	1.24	27.05	
35	3-6	1.3	2291 \pm 49	1.1	1274 \pm 46				27.36	
35	3-Total		3412 \pm 53		2204 \pm 51				27.54	-0.78 ± 0.14
36	5-4	2.0	76 \pm 11	1.8	77 \pm 10	38.00 ¹			25.88	0.02 ± 0.37
36	5-5	0.5	120 \pm 11	0.8	95 \pm 10				26.08	-0.42 ± 0.28
38	6-4	2.5	92 \pm 11			39.42	38.20		25.97	< -2.01 ± 0.64
39	4-1	1.9	84 \pm 11	1.7	36 \pm 10	38.43 ¹		2.47	25.93	-1.52 ± 0.57
39	4-4	1.1	46 \pm 11	0.03	282 \pm 10				25.67	3.26 ± 0.45
40	4-1	1.4	1215 \pm 25	1.0	487 \pm 10	39.18	37.68	6.48	27.09	
40	4-2	2.5	493 \pm 17	2.3	504 \pm 10				26.70	
40	4-Total		1708 \pm 30		991 \pm 14				27.24	-0.98 ± 0.13
41	4A-2	2.3	48 \pm 11			38.58	38.56	1.96	25.68	< -0.84 ± 0.73
43	4A-5	2.1	33 \pm 11	2.16	48 \pm 10	38.77 ¹		2.2	25.52	0.67 ± 0.72

¹ The luminosity for these sources is in the 0.1-10.0 keV band (from Table 1).

FIG. 1.— Adaptively smoothed images of the Antennae in the soft (0.3-2.0keV) and medium (2.0-4.0keV) bands. The discrete sources are represented by their 3σ source ellipses. The numbering convention is the same as in Table 1 of Paper II. Light blue ellipses indicate sources with an extended component, green ellipses indicate variable sources and black ellipses indicate highly obscured sources.

FIG. 2.— The composite spectra of the individual sources in the Antennae in the three different luminosity bins described in the text. In each figure the top panel shows the spectrum with the best fit model and the bottom panel shows the residuals after the fit. In the top left figure the dotted line shows the disk-BB model, the dashed line shows the PO component and the dash-dot line shows the RS component. In the top right figure the dashed line shows the disk-BB component, and the dotted and dash-dot line show the two RS components. In the bottom figure the dashed line shows the PO component and the dash-dot line shows the RS component.

FIG. 3.— HST-WFPC2 H α (a; top left), U (b; top right) and I (c; bottom left) band images of the Antennae showing the X-ray sources together with the optical sources. The arrow in the top left corner points towards the North. Yellow ellipses correspond to the 3σ positional ellipses of X-ray sources with luminosities above 10^{39} erg s $^{-1}$, green ellipses to sources in the $3 \times 10^{38} - 10^{39}$ erg s $^{-1}$ range and blue ellipses to sources below 3×10^{38} erg s $^{-1}$. The red symbols mark the bright optical sources from Whitmore et al. (1999) (X’s for young clusters, crosses for intermediate age clusters, diamonds for globular clusters and circles for foreground stars). (d) In the top panel we plot the offsets between the X-ray source and the most nearby optical counterpart from the papers of Whitmore et al. (1999) and Whitmore & Schweizer (1995) for the sources with luminosities above 10^{39} erg s $^{-1}$ (left) and between $3 \times 10^{38} - 10^{39}$ erg s $^{-1}$ (right). The vectors are proportional to the magnitude of the offset. The numbers give the sources ID. In the bottom panel we plot the offsets of the X-ray sources from the I-band optical sources detected down to a 7σ level (see text for details). The vectors for sources 12 and 14 extend beyond the left side of the image. The offsets of sources 13 and 14 are in the same direction.

FIG. 4.— Soft (left) and medium (right) band X-ray images of the Antennae with overlaid the X-ray and radio sources. Yellow, green and blue ellipses show the 3σ positional ellipses for X-ray sources with luminosities above 10^{39} erg s $^{-1}$, between 3×10^{38} and 10^{39} erg s $^{-1}$, and below 3×10^{38} erg s $^{-1}$, respectively. The red symbols correspond to the radio sources detected by Neff & Ulvestad (2000) (crosses and X’s mark flat and steep radio sources respectively). In the image North is up and East is left.

FIG. 5.— A VLA HI map of the Antennae (from Hibbard et al. 2001) with the position of the X-ray sources marked by their 3σ ellipses. The contours correspond to column densities of $(17.5, 87.5, 175.5, 262.5) \times 10^{22}$ cm $^{-2}$. (North is up and East is left).

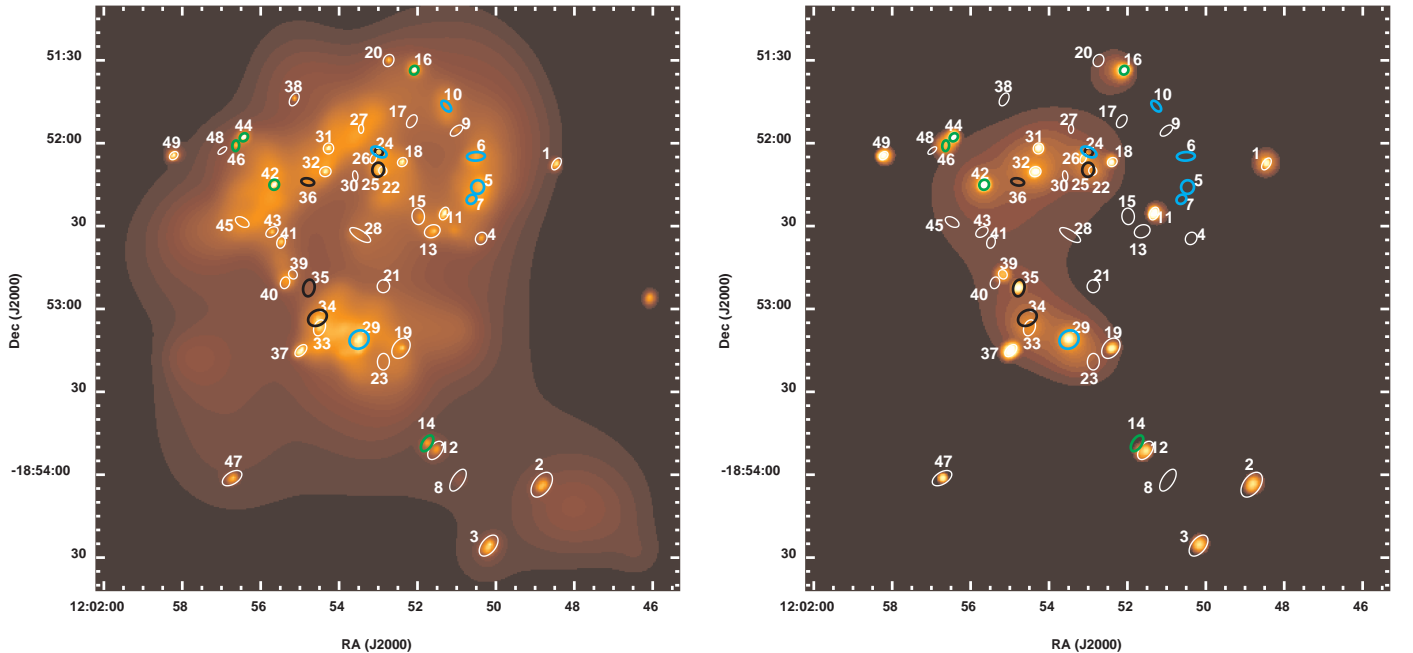


FIG. 1.—

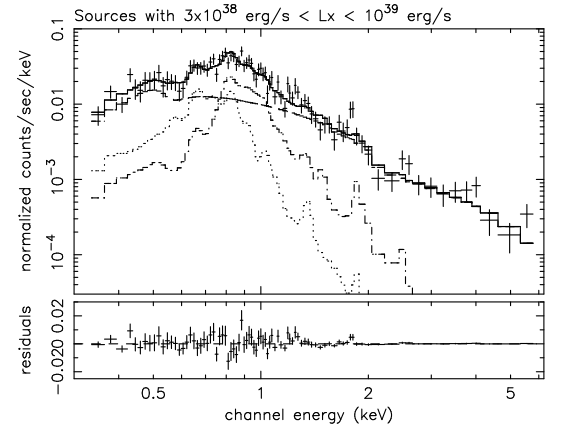
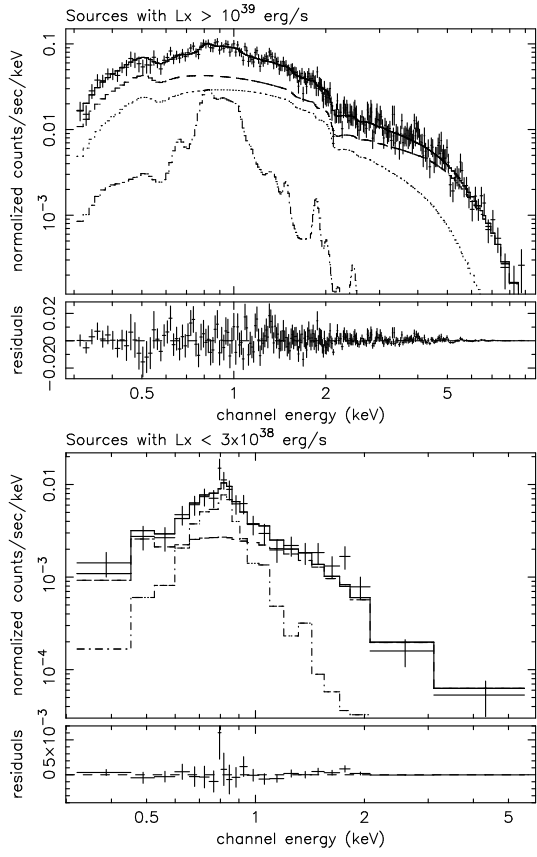


FIG. 2.—

FIG. 3.—

FIG. 4.—

FIG. 5.—

This figure "f3.jpg" is available in "jpg" format from:

<http://arxiv.org/ps/astro-ph/0203175v1>

This figure "f4.jpg" is available in "jpg" format from:

<http://arxiv.org/ps/astro-ph/0203175v1>

This figure "f5.jpg" is available in "jpg" format from:

<http://arxiv.org/ps/astro-ph/0203175v1>